Photochemistry and Photobiology, 2000, 71(4): 431–440

Development and Intercalibration of Ultraviolet Solar Actinometers

Joseph J. Jankowski[1], David J. Kieber*[1], Kenneth Mopper[2] and Patrick J. Neale[3]

[1]State University of New York, College of Environmental Science and Forestry, Department of Chemistry, Syracuse, NY;
[2]Washington State University, Department of Chemistry, Pullman, WA and
[3]Smithsonian Environmental Research Center, Edgewater, MD

Received 30 June 1999; accepted 21 January 2000

ABSTRACT

Ultraviolet (UV) sunlight actinometers were developed based on the photolysis of nitrate and nitrite. Photon exposures (*i.e.* time-integrated irradiances) were quantified from the photochemical production of salicylic acid (SA) or *p*-hydroxybenzoic acid (pHBA) formed by the reaction of the hydroxyl radical with benzoic acid. The solar response bandwidth for the nitrate actinometer in quartz tubing was 322 ± 11 nm during the Spring of 1999, while the response bandwidth of the Mylar D-filtered nitrite actinometer was 355 ± 25 nm. Intercomparisons of the nitrate and nitrite actinometers with a Smithsonian Environmental Research Center SR-18 scanning UV-B radiometer (SERC SR-18) and an Optronics OL-754 spectroradiometer (OL-754) were performed during the summer of 1998, and the winter and spring of 1999. Photon exposures determined by the nitrate actinometer were in excellent agreement with the SERC SR-18, with a slope (95% confidence interval [CI]) of 0.98 ± 0.01 based on SA production and 0.94 ± 0.02 based on pHBA production. Excellent agreement was also found between the nitrite actinometer and the OL-754, with a slope (95% CI) of 1.00 ± 0.01 using SA production and 1.00 ± 0.02 using pHBA production. These actinometers are well suited for use in the water column and are sufficiently sensitive to determine photon exposures below the 0.1% UV light-level.

INTRODUCTION

The ultraviolet (UV)† accounts for a small fraction of the total solar radiation reaching the Earth's surface. This region of the solar spectrum (290–400 nm), however, has a strong impact on photochemical and photobiological processes, especially in aquatic systems (1–3). Thus, accurate quantification of UV irradiance is critical for determining the effects of UV on aquatic systems. However, this quantification is difficult because the intensity and spectral distribution of UV are affected by numerous physical and chemical processes in both atmospheric and aquatic systems.

UV irradiance fluctuates daily and seasonally as a function of latitude, solar zenith angle, cloud cover (4–7) and stratospheric ozone concentration (8). The UV irradiance also varies greatly as a function of depth in the water column, depending primarily on the concentration of dissolved organic matter (DOM) and phytoplankton (9–14). Characterization of UV irradiance is difficult, as it can vary by more than five orders of magnitude. Consequently, instrumentation to quantify the UV irradiance and photon exposure must be very sensitive, reject stray light and provide a wide linear dynamic range (7,15).

Current methods for quantifying UV irradiance include spectral instruments, broadband instruments, chemically based actinometers and biologically based dosimeters. Spectroradiometers are the primary tool for measuring UV irradiance at the Earth's surface. They can be used to interpret changes in the UV spectrum because they measure spectral intensities over an adjustable, near-continuous wavelength range. When spectral scans are performed, irradiance data can be integrated to yield the photon exposure, which is defined by the International Union of Pure and Applied Chemistry as the irradiance integrated over the time of irradiation (16). However, measurement of the photon exposure in the UV-B (290–320 nm) is often inaccurate because of rapid temporal variations in UV-B on a time-scale that is faster than a spectral scan, and because low levels of UV-B can provide a signal near the background dark current of the instrument (7,15,17). Recent development of a rapidly scanning UV-B radiometer (17) allows for better measurement of the irradiance and photon exposure in the UV-B, while still providing some spectral resolution. Disadvantages of spectral instruments are that they are expensive, often temperature dependent and typically have a slow response time (*ca* 1 scan per 10 min).

Broadband instruments, such as the Robertson–Berger meter (18,19), measure the photon exposure over a specific wavelength range and are inexpensive compared to spectroradiometers. However, broadband instruments lack spectral resolution, are difficult to calibrate and, like spectroradiometers, their response is temperature dependent (20). More importantly, except for a few spectroradiometers specifically

*To whom correspondence should be addressed at: State University of New York, College of Environmental Science and Forestry, Department of Chemistry, 1 Forestry Drive, Syracuse, NY 13210, USA. Fax: 315-470-6856; email: djkieber@mailbox.syr.edu

†*Abbreviations:* CI, confidence interval; CV, coefficient of variation; DOM, dissolved organic matter; HPLC, high-performance liquid chromatography; OL-754, Optronics OL-754 spectroradiometer; pHBA, *p*-hydroxybenzoic acid; PMT, photomultiplier tube; SA, salicylic acid; SERC SR-18, Smithsonian Environmental Research Center SR-18 scanning radiometer; UV, ultraviolet.

designed for underwater irradiance measurements (*e.g.* LI-COR LI-1800UW spectroradiometer), most instrumental methods are not suited for *in situ* water column irradiance measurements and long-term (daylong) underwater deployments at multiple depths.

An alternate approach to characterize the irradiance in natural waters involves the use of chemical actinometers or biological dosimeters. Actinometers or dosimeters are based on photochemical reactions in solutions (21–23) and films (24), or the photoreaction of biologically based molecules (*e.g.* DNA) (25,26) or organisms (27,28). Chemical actinometers measure the photon exposure (16) over a defined wavelength range based on their sunlight response (*vide infra*), whereas biological dosimeters quantify the effects of sunlight on organisms over a defined action spectrum. Chemical actinometers and biological dosimeters do not provide wavelength-dependent information, but they are very inexpensive compared to instruments, and because they continually measure the irradiance within the reaction vessel, they are particularly useful for determining the scalar photon exposure in the water column. Because most photoprocesses are not dependent on the direction of solar radiation, the scalar photon exposure is a better parameter to quantify photochemical and photobiological processes compared to the downwelling photon exposure (*i.e.* time-integrated downwelling irradiance) (6). Additionally, multiple actinometers and dosimeters can be simultaneously deployed to integrate the photon exposure throughout a water column, providing spatial and temporal characterization that is not easily achieved by instrumental methods.

In this paper, we introduce two broadband sunlight actinometers that are based on the photolysis of nitrate (29–34) and nitrite (32,35–37). The primary reactive intermediate of nitrate and nitrite photolysis, the hydroxyl radical, reacts with benzoic acid leading to the formation of monohydroxybenzoic acids (38), including SA or pHBA (39). The wavelength and temperature-dependent quantum yields for the production of SA and pHBA from nitrate and nitrite photolysis and algorithms for determination of spectral radiant fluxes are given in Jankowski *et al.* (39). Quantum yields were used in the present report to determine solar UV photon exposures. Development of these solar actinometers included determination of the response bandwidth for nitrate and nitrite, and intercomparison with two spectral instruments, a Smithsonian Environmental Research Center SR-18 scanning radiometer (SERC SR-18) and an Optronics OL-754 spectroradiometer (OL-754).

MATERIALS AND METHODS

Chemicals. Sodium nitrate (≥99.995%), and pHBA (≥99%) were obtained from Aldrich Chemical Company (Milwaukee, WI). Sodium nitrite (>99%) was purchased from Fluka Chemical (Buchs, Switzerland). SA (≥99.5%) and reagent grade sodium bicarbonate, benzoic acid, monobasic potassium phosphate and phosphoric acid were purchased from J.T. Baker, Inc. (Phillipsburg, NJ). Distilled-in-glass high purity methanol was obtained from Baxter Diagnostics, Inc. (McGaw Park, IL). All chemicals were used as received, except for benzoic acid, which was recrystallized three times from high-purity laboratory water.

All solutions were prepared with water from a Millipore water purification system (Millipore Corp., Chicago, IL) having a specific resistance greater than 18 MΩ cm. The water-purification system consisted of filtration/dechlorination cartridges followed by a Milli-RO (reverse osmosis) system, a four-cartridge Milli Q system (Super C carbon cartridge, two ion-exchange cartridges and an Organex Q cartridge) and final filtration through a 0.2 μm Whatman Polycap AS capsule (Fisher Scientific, Springfield, NJ). All solutions were prepared in borosilicate glassware and stored in the dark at 4°C.

Nitrate and nitrite actinometers. The actinometers consisted of 1 m*M* sodium nitrite or 10 m*M* sodium nitrate in a 1 m*M* benzoic acid solution buffered with 2.5 m*M* sodium bicarbonate. The pH of the actinometers was 7.2. These solutions were stable for at least 45 days when stored in the dark and refrigerated.

Analyte quantification. Quantification of the photochemical products, SA and pHBA, was performed according to the procedures outlined in Jankowski *et al.* (39). Briefly, SA and pHBA were quantified by reverse-phase high-performance liquid chromatography (HPLC) with fluorescence detection of SA using an F-1050 Hitachi fluorometer (Hitachi Instruments, Inc., Danbury, CT) at an excitation wavelength of 305 ± 7.5 nm and an emission wavelength of 410 ± 7.5 nm. pHBA was quantified at 250 nm using a Shimadzu SPD-10AV absorbance detector (Shimadzu Scientific Instruments, Inc., Columbia, MD). Peak areas (SA) and heights (pHBA and mHBA) were determined using ELAB integration software (OMS Tech, Inc., Miami, FL). Calibration curves were generated by standard additions of the stock solution to the actinometer solution, with final concentrations ranging from 50 to 2000 n*M*. The detection limit of this method, with a signal-to-noise ratio of two, was typically 0.5 n*M* for SA and 5 n*M* for pHBA. Detection limits were primarily dependent on the purity of the benzoic acid.

Photodegradation of SA. SA can undergo direct photolysis in the UV-B and at shorter wavelengths of the UV-A (39). To account for the degradation of SA during daylong irradiations, the quantum yield for the direct photolysis of SA was determined at 10 nm intervals from 290 to 330 nm. Degradation of SA was performed in a 1 cm quartz cuvette with 3.0 mL of an air-saturated actinometer solution containing 2 μ*M* SA but no nitrate or nitrite. For all wavelengths except 330 nm, quantum yield measurements were performed with an ISS PC1 photon-counting spectrofluorometer (Champaign, IL) equipped with a 300 W xenon lamp. At 330 nm it was not possible to detect a loss in fluorescence using the scanning fluorometer. Therefore, the quantum yield at this wavelength was determined using a 1000 W xenon lamp with a GM 252 high intensity quarter meter grating monochromator and an enclosed temperature-controlled sample chamber (Spectral Energy Corp., Westwood, NJ). All quantum yields were determined at 25°C, except for the temperature-dependence study. The spectral radiant flux (16) inside the quartz cell, P_λ, was determined using potassium ferrioxalate actinometery (40). Wavelength-dependent quantum yields for SA degradation were determined from the first-order rate equation for SA degradation, which is valid under optically thin conditions (abs < 0.01 at λ ≥ 290 nm):

$$\left(\frac{-\mathrm{d[SA]}}{\mathrm{dt}}\right)_\lambda = 2.303\epsilon_\lambda\Phi_\lambda P_\lambda \ell V^{-1}[\mathrm{SA}] \qquad (1)$$

where [SA] is the concentration of SA (*M*), ϵ_λ is the molar absorption coefficient for SA ($cm^2\ mol^{-1}$, Table 1), Φ_λ is the quantum yield for SA photolysis (mol $einstein^{-1}$), P_λ is the spectral radiant flux (einstein min^{-1}), ℓ is the pathlength of the quartz cuvette (cm) and V the volume of the irradiated solution (mL). After Eq. 1 was integrated with respect to time, quantum yields were determined from the slope of the linear plot of the natural logarithm of [SA] *versus* time, where the slope equals $2.303\epsilon_\lambda\Phi_\lambda P_\lambda \ell V^{-1}$.

Spectral instruments. The SERC SR-18 radiometer (Smithsonian Environmental Research Center, Edgewater, MD) measures the solar UV irradiance at fixed wavelengths selected by 18 narrow bandpass interference filters from 290 to 330 nm. The filters have bandwidths that average 2.2 nm (range of 2–2.5 nm) as determined by a Cary 4 spectrophotometer. The filters are located on a wheel that has a rotational frequency of 15 min^{-1}. Radiation is detected by a solar-blind photomultiplier tube (PMT) after passage through a Teflon diffuser, a narrow bandpass filter and a three-aperture collimating device. The PMT is temperature controlled at 23°C and operates in the current mode. The output current is converted to voltage and averaged for 1 min per filter. Calibration of the spectral responsivity was performed at the Smithsonian Environmental Research Center

with a 1 kW NIST-traceable FEL-type quartz-halogen lamp. Frequent sampling, in conjunction with measurement of two dark channels per rotation, makes this instrument ideal for determination of time-integrated UV-B irradiances. Further details of the instrument are available, including extensive intercalibration with numerous spectroradiometers (17,41).

The OL-754 spectroradiometer (Orlando, FL) contains a high-sensitivity, temperature-stabilized, S-20 response PMT and utilizes a double monochromator to minimize stray light. A waterproof fiber-optic probe with cosine response was employed as the input optic for scans between 290 and 500 nm taken at 1 nm intervals, with an average scan time of 11 min. A 2 nm bandwidth was selected for spectral measurements. The instrument was calibrated with a 1 kW NIST-traceable FEL-type quartz-halogen lamp.

Intercalibration study. Photon exposure measurements were made on the rooftop of Baker Laboratory (State University of New York, College of Environmental Science and Forestry, Syracuse, NY) during the summer of 1998, and the winter and spring of 1999. Actinometer solutions were deployed in quartz tubing (<30 cm in length, 20 mm i.d. × 24 mm o.d.) that was sealed with virgin TFE Teflon end fittings. The Teflon stoppers allowed sampling of the actinometers without the introduction of headspace into the solutions (42). The nitrate actinometer was deployed alongside the SERC SR-18 UV-B scanning radiometer from 4–11 February, on 16 February and on 2 March 1999. The nitrate actinometer was deployed alongside the OL-754 from 23–25 March 1999, in addition to an earlier summer deployment on 22 July 1998. The nitrite actinometer was compared to the OL-754 from 17–21 February, 24–26 February and on 1 March 1999. The actinometer solutions and spectral instruments were placed on an all-black platform in an unshaded region of the roof. The actinometer solutions were placed in a circulating water bath to maintain a constant temperature. The underside of the shallow water bath (*i.e.* 3 cm high) was painted flat black to minimize reflection. The mean temperature in the water bath was 10 ± 2°C over the entire intercalibration study, except for July 1998, when the temperature was 20°C. Actinometer deployments ranged from 4.5 to 6 h, with 6 to 9 time points taken per day. Spectral measurements were made with the SERC SR-18 or the OL-754 throughout an experiment at 4 s and 11 min intervals, respectively.

Photon exposures determined with the actinometers were correlated to the instrumentally determined photon exposures. The best-fit line and y-intercept were determined using the major axis correlation method of Pearson (43). This method was chosen because it accounts for error in the instruments and actinometers.

Light focusing experiment. An experiment was conducted to determine if the quartz tubing focused or attenuated sunlight when deployed in water. Three quartz tubes and three uncovered Petri dishes (Pyrex, 14 cm diameter, 2 cm high) containing the nitrate actinometer were exposed to midday sunlight for 4 h on the Baker Laboratory rooftop. This experiment was performed in a shallow, circulating water bath that maintained the temperature at 20 ± 1°C. Aliquots of the actinometer solution were taken from the quartz tubes and Petri dishes at five time points and analyzed for SA production.

RESULTS

Light focusing experiment

Before the actinometers were used to quantify photon exposures, an experiment was conducted to determine the production of SA in submerged quartz tubing relative to its production in three uncovered Petri dishes. In this experiment, the photon exposure was 11.6 μeinstein cm^{-2} over the 311–333 nm bandwidth of the nitrate actinometer. A plot of the SA production in the Petri dishes relative to the quartz tubing yielded a slope (95% confidence interval [CI]) of 1.02 ± 0.10 and a y-intercept (95% CI) of −25.9 ± 88.5 n*M*. The slope and y-intercept were not significantly different from 1 and 0, respectively, at the 95% confidence level (as determined by the correlation method of Pearson (43)), indicating that passage of solar radiation through the quartz tubing did not magnify or attenuate solar UV irradiance. Thus, no correction was needed to determine photon exposures when the actinometers were deployed in submerged quartz tubes.

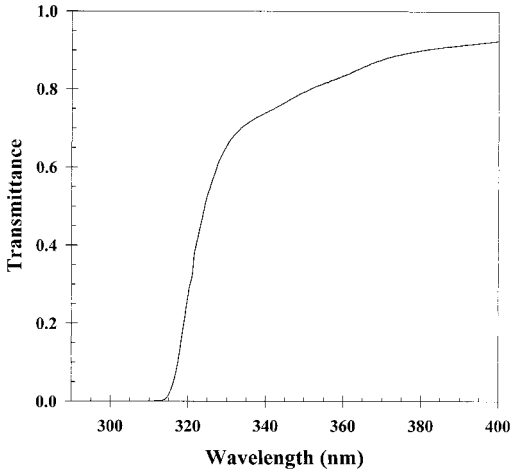

Figure 1. Transmittance of Mylar D in Milli Q water.

Mylar D filter

Mylar D (0.16 mm thickness) is an inexpensive, readily available long bandpass filter that was used with the nitrite actinometer to attenuate UV-B radiation (Fig. 1). It was wrapped around the quartz tubes, and a thin strip of black tape was used to secure the Mylar D to the tubing. The Mylar D filter greatly reduced the degradation of SA, as SA degrades primarily in the UV-B (*vide infra*). Additionally, Mylar D shifted the spectral response of nitrite toward longer wavelengths, thereby minimizing the overlap of the response bands of the nitrate and nitrite actinometers. Mylar D degrades slowly with solar exposure (J.J. Jankowski *et al.*, unpublished), altering its transmittance. Therefore, the Mylar D filter was replaced every few days during the intercomparison study.

Quantum yield for SA degradation

The quantum yield for SA degradation at 25°C exhibited negligible wavelength dependence from 290 to 330 nm (Fig. 2), with a mean value (95% CI) of 0.0114 ± 0.0007. The lowest quantum yield (95% CI) was at 290 nm (0.00969 ± 0.00128) and the highest value was at 330 nm (0.0139 ± 0.0041). Neither of these quantum yields was significantly different from the mean value at a 95% CI. As expected, the primary photolysis of SA was not temperature dependent. Irradiations at 310 nm and 10, 20 and 30°C yielded the same quantum yield (95% CI) (0.0114 ± 0.0004).

Solar response of the nitrate and nitrite actinometers

The solar response of the actinometers was determined so that they could be used to quantify photon exposures. Under the optically thin conditions used in our study (absorbance <0.05 at λ ≥ 310 nm), the wavelength-dependent photochemical production of SA or pHBA from nitrate or nitrite photolysis can be determined by:

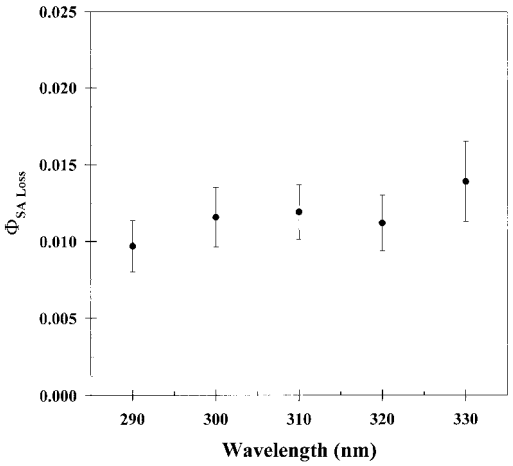

Figure 2. Wavelength-dependent quantum yield for SA degradation in a 2.5 m*M* bicarbonate solution containing 2 μ*M* SA and 1 m*M* benzoic acid. Error bars denote the 95% CI (n = 5–11). Quantum yields for SA degradation are presented in a tabular form by Jankowski (48).

$$\left(\frac{d[A]}{dt}\right)_\lambda = 2.303\epsilon_\lambda\Phi_\lambda T_\lambda E_\lambda[NO_x^-] = k_1[NO_x^-] \qquad (2)$$

where [A] is the concentration of SA or pHBA (*M*), Φ_λ is the quantum yield for SA or pHBA formation from nitrate or nitrite photolysis (mol einstein^{-1}) (39), T is the transmittance of Mylar D (this factor is only needed when Mylar D is used as a filter for the quartz tubing), E_λ is the spectral irradiance (einstein cm^{-2} nm^{-1} s^{-1}), ϵ_λ is the wavelength-dependent molar absorption coefficient of nitrate or nitrite (cm^2 mol^{-1}) and [NO_x^-] is the concentration of nitrate or nitrite in the actinometer (*M*). The first-order rate constant, k_1, was calculated using wavelength-dependent values of the molar absorption coefficient (Table 1), the quantum yield for SA or pHBA production (Table 2), experimentally determined values of T (Fig. 1) and the average daytime spectral irradiance measured during rooftop irradiations with the OL-754 in the Spring of 1999. To determine the solar response of the actinometers, k_1 was plotted as a function of wavelength (Fig. 3). The mean-response wavelength of the actinometers in sunlight was then determined by integrating the area under the response curve and calculating the wavelength that corresponds to half of the area. The response bandwidth was determined as the width at half-height of the response curve.

The response bandwidth of the nitrate actinometer was 311–333 nm, with a mean response at 322 nm (Fig. 3A), while the response bandwidth in the Mylar D-filtered nitrite actinometer was 330–380 nm, with a mean response at 355 nm (Fig. 3B). The response bandwidth for nitrite in quartz tubing (with no Mylar D) was 325–377 nm and the mean-response wavelength was 352 nm (data not shown). The response bandwidth for SA degradation in the nitrate actinometer was determined from a plot of the first-order rate constant for SA loss as a function of wavelength (Fig. 4). This rate constant is the product of the OL-754 average daytime spectral irradiance in Spring 1999, the molar absorption coefficient for SA (Table 1) and the quantum yield for SA degradation (*vide supra*). From the integration of its response area, the response bandwidth for SA degradation in sunlight was 308–327 nm, with a mean response at 318 nm.

Table 1. Molar absorption coefficients (10^3 cm^2 mol^{-1}) for nitrate, nitrite and salicylic acid in the actinometer solutions as a function of wavelength (nm)

λ	$\epsilon_{NO^{3-}}$	$\epsilon_{NO^{2-}}$	ϵ_{SA}	λ	$\epsilon_{NO^{3-}}$	$\epsilon_{NO^{2-}}$	ϵ_{SA}	λ	$\epsilon_{NO^{2-}}$
290	5.58	8.79	3183	334	0.46	15.85	70.9	378	11.14
291	5.79	8.84	3277	335	0.39	16.30	63.4	379	10.40
292	5.99	8.88	3359	336	0.32	16.75	56.1	380	9.69
293	6.18	8.91	3430	337	0.27	17.22	49.2	381	8.96
294	6.36	8.93	3484	338	0.23	17.67	44.2	382	8.26
295	6.53	8.95	3522	339	0.19	18.14	39.0	383	7.58
296	6.68	8.97	3539	340	0.16	18.59	33.3	384	6.93
297	6.81	8.98	3534	341	0.13	19.04	29.2	385	6.31
298	6.92	9.00	3510	342	0.11	19.48	25.2	386	5.61
299	7.01	9.01	3465	343	0.09	19.92	21.3	387	5.06
300	7.08	9.03	3402	344	0.08	20.32	17.8	388	4.53
301	7.12	9.04	3324	345	0.06	20.71	14.4	389	4.06
302	7.14	9.07	3231	346	0.05	21.08	11.0	390	3.70
303	7.12	9.10	3121	347	0.04	21.42	9.3	391	3.28
304	7.08	9.14	2998	348	0.04	21.72	7.6	392	2.88
305	7.01	9.19	2861	349	0.03	21.99	6.0	393	2.53
306	6.91	9.24	2707	350	0.03	22.22	4.9	394	2.22
307	6.78	9.31	2541	351		22.41	2.9	395	1.93
308	6.62	9.37	2359	352		22.56	1.9	396	1.67
309	6.43	9.45	2172	353		22.67	1.4	397	1.44
310	6.23	9.53	1982	354		22.73	1.0	398	1.22
311	5.99	9.61	1789	355		22.73	0.9	399	1.05
312	5.74	9.71	1606	356		22.68	0.7	400	0.89
313	5.46	9.83	1431	357		22.58	0.5	401	0.75
314	5.18	9.95	1271	358		22.45	0.3	402	0.64
315	4.88	10.09	1122	359		22.28	0.1	403	0.53
316	4.57	10.24	985	360		22.05		404	0.44
317	4.26	10.41	862	361		21.76		405	0.37
318	3.94	10.60	747	362		21.39		406	0.31
319	3.63	10.81	646	363		20.95		407	0.26
320	3.31	11.03	552	364		20.48		408	0.21
321	3.01	11.27	471	365		19.99		409	0.17
322	2.72	11.53	399	366		19.45		410	0.14
323	2.44	11.81	339	367		18.86		411	0.12
324	2.16	12.10	287	368		18.22		412	0.10
325	1.91	12.40	243	369		17.58		413	0.08
326	1.67	12.73	207	370		16.94		414	0.06
327	1.46	13.06	178	371		16.28		415	0.05
328	1.26	13.42	153	372		15.61		416	0.04
329	1.08	13.79	133	373		14.91		417	0.03
330	0.89	14.17	117	374		14.17		418	0.03
331	0.75	14.57	102	375		13.40		419	0.02
332	0.64	14.98	89.9	376		12.65		420	0.02
333	0.54	15.41	79.4	377		11.89			

The nitrate actinometer response bandwidth varied slightly with respect to season. When the nitrate response bandwidth determined for SA or pHBA in Syracuse, NY during the summer of 1998 (311–333 nm) was compared to the response bandwidth determined during Winter/Spring 1999 (310–334 nm), we observed a 2 nm increase in the response bandwidth and a 1 nm shift in the mean response wavelength from 322 to 323 nm. In contrast, the nitrite actinometer response bandwidth and mean response wavelengths were the same for both the summer and winter/spring studies. Within a season, the response bandwidths and mean-response wavelengths of the actinometers did not change significantly during the intercomparison studies in Syracuse, NY for weather conditions that varied from snow flurries to cloudless, sunny days. Although the bandwidths and mean-response wave-

Table 2. Average quantum yields for SA and pHBA production at 25°C from nitrate or nitrite photolysis in a pH 7.2 solution of 1.0 m*M* benzoic acid and 2.5 m*M* bicarbonate buffer

Nitrate			Nitrite		
λ (nm)	Φ_{SA} (%)	Φ_{pHBA} (%)	λ (nm)	Φ_{SA} (%)	Φ_{pHBA} (%)
290	0.250	0.181	290	0.633	0.379
295	0.192	0.126	295	0.564	0.360
300	0.172	0.119	300	0.526	0.351
305	0.149	0.105	310	0.422	0.285
310	0.146	0.101	320	0.356	0.216
315	0.150	0.106	330	0.337	0.198
320	0.164	0.106	340	0.266	0.173
325	0.196	0.132	350	0.222	0.134
330	0.241	0.161	360	0.187	0.118
335	0.305	0.193	370	0.185	0.120
340	0.358	0.211	380	0.184	0.108
345	0.439	0.238	390	0.230	0.125
350	0.418	0.345	400	0.280	0.183
			405	0.322	0.195

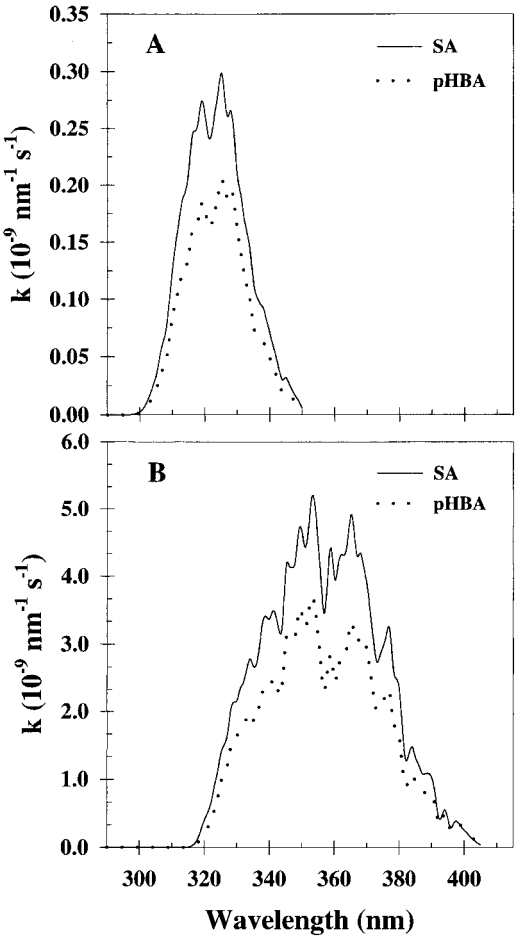

Figure 3. First-order rate constant for the photochemical production of SA and pHBA from (A) nitrate photolysis in quartz tubing and (B) nitrite photolysis in Mylar D-filtered quartz tubing, plotted as a function of wavelength.

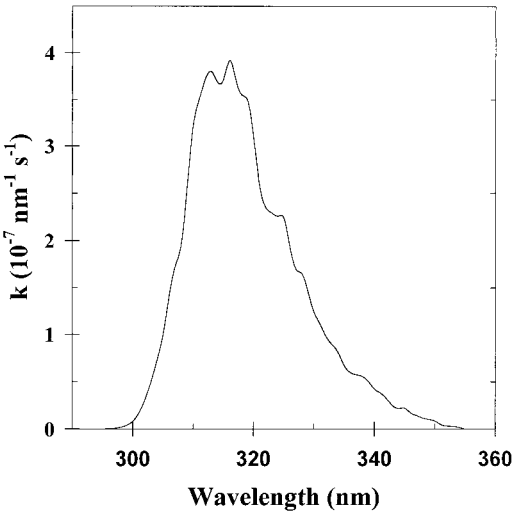

Figure 4. First-order rate constant for SA degradation in quartz tubing plotted as a function of wavelength.

lengths changed very little during this study, irradiances did vary considerably. However, variations in the irradiance will not affect the calculation of the photon exposure in Eqs. 3 and 5, unless large, unequal variations in the spectral irradiance are observed within the bandwidth of the actinometer.

Changes in the solar spectrum resulting from large latitudinal changes will also affect the response bandwidths and mean-response wavelengths of the actinometers. For example, the latitudinal change in the response of the nitrate actinometer under clear, summertime conditions was determined from GCSOLAR model (44) daily photon-exposure estimates (Fig. 5). Enrichment in the UV-B at lower latitudes caused the response bandwidth of the nitrate actinometer to shift to shorter wavelengths by 1–2 nm based on integration of the area under the curve. Because the spectral distribution of UV-A is not affected by latitudinal changes as strongly as UV-B, the response bandwidth of the nitrite actinometer

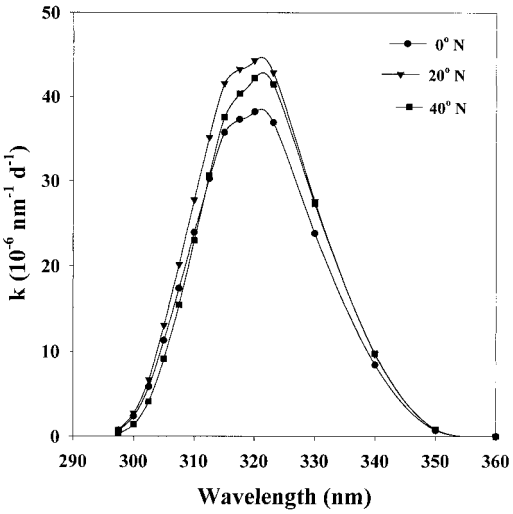

Figure 5. Latitudinal response of the first-order rate constant for SA production from nitrate photolysis in quartz tubing plotted as a function of wavelength, based on clear sky, summertime (July) daily photon exposure values at 0, 20 and 40°N.

Table 3. Values of parameters used in Eqs. 3 and 5 to determine photon exposures during the Spring 1999 study in Syracuse, NY. Values for ϵ_{avg}, Φ_{avg} and ϵ_{SA} are the average values over the nitrate and Mylar-D nitrite response bandwidths, 311–333 nm and 330–380 nm, respectively. Values of Φ_{avg} are only valid at 283 K. For other temperatures, use Eq. 6 to calculate Φ_{avg}

	Nitrate actinometer		Nitrite actinometer	
	SA	pHBA	SA	pHBA
ϵ_{avg} (cm^2 mol^{-1})	2.89×10^3	2.89×10^3	1.93×10^4	1.93×10^4
$\Phi_{avg,\ 283\ k}$	1.48×10^{-3}	1.08×10^{-3}	1.42×10^{-3}	9.26×10^{-4}
E_A (kJ mol^{-1})	15.8	16.8	13.9	15.3
T			0.78	0.78
ϵ_{SA} (cm^2 mol^{-1})	1.02×10^6			
Φ_{SA}	1.20×10^{-2}			
f	0.61			

did not vary significantly with latitude. Although no major spectral shifts were noted here, solar responses of nitrate and nitrite, relevant to the study site under consideration, should be determined using spectroradiometric data or GCSOLAR model data (44).

Once quantum yields of the actinometers and their solar response bandwidths were known, photon exposures were determined from the photochemical production of SA or pHBA:

$$E_P = \frac{[A]}{2.303T\Phi_{avg}\epsilon_{avg}[NO_x^-]} \quad (3)$$

where E_P is the photon exposure (einstein cm^{-2}), [A] is the concentration of SA or pHBA produced in the actinometer solution (*M*) during the irradiation, T is the mean transmittance of Mylar D over the nitrite actinometer solar response bandwidth (for quartz this factor is not needed), Φ_{avg} the mean quantum yield for SA or pHBA production over the response bandwidth of the actinometer (mol $einstein^{-1}$), ϵ_{avg} the mean molar absorption coefficient for nitrate or nitrite over the solar response bandwidth of the actinometer (cm^2 mol^{-1}) and $[NO_x^-]$ is the concentration of nitrate or nitrite in the actinometer solution (*M*). Values of the parameters used in Eq. 3 are presented in Table 3. Concentrations of NO_x^- in the actinometers did not vary during daylong irradiations (as determined by spectrophotometry), and they are substantially greater than concentrations of products (*e.g.* 10 m*M versus* 1 μM). Therefore, $[NO_x^-]$ is treated as a constant in this study.

For long-term irradiations of the nitrate actinometer, photon exposures can be determined by integrating the rate law for net SA production, which is equal to the total production of SA from nitrate photolysis minus the loss of SA due to its photodegradation:

$$\frac{d[SA]}{dt} = 2.303\epsilon_{avg}\Phi_{avg}E[NO_3^-] - 2.303\epsilon_{SA}\Phi_{SA}E_{SA}[SA] \quad (4)$$

where ϵ_{avg} is the mean molar absorption coefficient of nitrate in its solar response bandwidth (cm^2 mol^{-1}), Φ_{avg} is the mean quantum yield for SA production in nitrate's solar response bandwidth (mol $einstein^{-1}$), E is the irradiance integrated over the bandwidth of the nitrate actinometer (einstein cm^{-2} s^{-1}), $[NO_3^-]$ is the concentration of nitrate (*M*), ϵ_{SA} is the mean molar absorption coefficient for SA in the SA degradation bandwidth (cm^2 mol^{-1}), Φ_{SA} is the quantum yield for SA degradation (mol $einstein^{-1}$), E_{SA} the irradiance integrated over the SA degradation bandwidth (einstein cm^{-2} s^{-1}) and [SA] is the concentration of SA(M). Values used in Eq. 3 for Φ_{avg}, ϵ_{avg}, Φ_{SA} and ϵ_{SA} are presented in Table 4 along with the average value of the activation energy, E_A, for SA production in the nitrate actinometer.

If we use spectroradiometric data to estimate the fraction, *f*, of solar radiation available in the SA degradation response bandwidth relative to the nitrate actinometer response bandwidth (Table 3), then Eq. 4 can be integrated to yield an equation for photon exposure that accounts for SA degradation in the nitrate actinometer (where $E_{SA} = f\,E$):

$$E_P = \frac{-1}{2.303f\epsilon_{SA}\Phi_{SA}}\ln\frac{((\epsilon_{avg}\Phi_{avg}[NO_3^-]) - f(\epsilon_{SA}\Phi_{SA}[SA]_t))}{((\epsilon_{avg}\Phi_{avg}[NO_3^-]) - f(\epsilon_{SA}\Phi_{SA}[SA]_0))} \quad (5)$$

where the initial and final concentrations of SA are $[SA]_0$ and $[SA]_t$, respectively. The parameter *f* (determined from OL-754 measurements in Syracuse, NY) is included because the daily photon exposure in the nitrate response bandwidth (311–333 nm) is 61% greater than in the SA degradation bandwidth (308–327 nm). If this term is not included, then the SA degradation will be overestimated, leading to an overestimation in the photon exposure using the nitrate actinometer. Photon exposures were quantified during long-term irradiations of the nitrate actinometer using values in Table 3. Equation 5 provides an accurate means for estimating photon exposures based on SA production during long-term deployments (*ca* >3 h) of the nitrate actinometer (*vide infra*). However, because pHBA undergoes very little photolysis in sunlight, long-term photon exposures using the nitrate actinometer are more easily quantified based on pHBA production using Eq. 3, if HPLC analyses are performed. During short-term deployments or deployments at depth in the water column, photon exposures should be determined based on SA production because its detection by fluorescence is inherently more sensitive than detection of pHBA by absorption (*vide infra*).

Uncertainty estimates

Uncertainties in the actinometers are due to three factors: uncertainties in the parameters used in Eqs. 3 and 5, uncertainty due to temperature fluctuations, and uncertainty (due to miscalculation) of the actinometers' response bandwidths. All of these individual errors are less than 10%.

Uncertainties inherent in experimentally determined quantum yields, molar absorption coefficients and concentrations of SA, pHBA or nitrate are minor. Quantum yields determined for SA production (39) have a percent coefficient of variation (%CV) of 7.4% in the response bandwidth of the nitrate actinometer and 4.5% in the response bandwidth of the nitrite actinometer. The mean errors are similarly small for determination of the molar absorption coefficients of nitrate (1.9% (45)) and nitrite (0.75% (46)) using UV spectrophotometry. For analyte productions greater than 100 n*M*, the %CV corresponding to product analyses by HPLC are less than 2%. Finally, the uncertainty in the nitrate concentration is a function of the accuracy and precision with which the actinometer solutions are made. Propagation analysis of the errors in Eqs. 3 or 5 yields a photon exposure uncertainty of 3.6% for the nitrate actinometer and 2.7% for the nitrite actinometer.

Although careful deployment of the actinometer solutions is important, the experimental protocol is very robust. The primary source of error during an experiment is fluctuation of the actinometer temperature. For example, a 2°C change in temperature during an experiment using a water bath will result in an error of approximately 3% if the temperature change is not taken into account. Because the photochemical production of SA and pHBA are temperature dependent (32,39), the solution temperature should be held constant and/or recorded. If the temperature of the actinometer changes during the course of a deployment, Eq. 6 can be used to determine the correct quantum yield to be used in Eqs. 3 and 5:

$$\Phi_{T1} = \Phi_{283K}\exp\left(\frac{E_A}{R}\left[\frac{1}{283} - \frac{1}{T_1}\right]\right) \quad (6)$$

where Φ_{T1} is the quantum yield at the new temperature, T_1, Φ_{283K} is the average quantum yield for SA or pHBA production in the nitrate or nitrite actinometers at 283 K (Table 3), E_A is the activation average energy for SA or pHBA production in the nitrate or nitrite actinometers (Table 3) and R the universal gas constant.

As previously noted, seasonal and latitudinal changes can affect actinometer response bandwidths. Consequently, there is some uncertainty in using the actinometers to determine photon exposures due to the assignment of the response bandwidths. Ideally, response bandwidths are determined using spectral irradiance data from spectroradiometric measurements (*vide supra*). Although the calculation of the response bandwidth is a straightforward process, miscalculations of the bandwidths can lead to under- or over-estimation of photon exposures. Accurate determination of the nitrate actinometer response bandwidth is particularly important because the spectral irradiance increases exponentially over a relatively narrow wavelength range. In contrast, accurate assessment of the nitrite actinometer response bandwidth is not as critical because the nitrite actinometer's bandwidth is approximately 50 nm and the spectral irradiance is relatively constant in the UV-A. If the response bandwidth of the nitrate actinometer was improperly calculated as 311–332 nm rather than 311–333 nm, then this would result in a 5% overestimation of the photon exposure. However, for the nitrite actinometer, a 1 nm bandwidth underestimation of 330–379 nm would result in a photon exposure overestimation of approximately 2%. When Eq. 5 is used to account for SA degradation, an additional source of error exists due to the uncertainty in the *f* parameter. The extent of this error is a function of the photochemical SA production. For example, a 10% underestimation of the *f* parameter will result in a 10% overestimation of the photon exposure at a SA production of 1000 n*M*. To minimize errors due to changes in bandwidths, spectroradiometric data or data from solar models (*e.g.* GCSOLAR (44)) should be used to determine the solar response bandwidths of the actinometers at the study site under consideration.

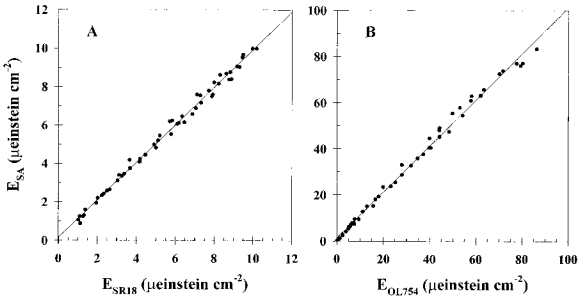

Figure 6. Photon exposure: (A) from 311 to 333 nm determined from the production of SA (Eq. 3, uncorrected for SA photolysis) in the nitrate actinometer correlated with photon exposures obtained using the SERC SR-18 radiometer. The coefficient of determination (r^2) was 0.99, the slope (±95% CI) was 0.98 ± 0.01, and the y-intercept (95% CI) was 0.14 ± 0.14 μeinstein cm^{-2}; and (B) from 330 to 380 nm determined from the production of SA in the nitrite actinometer (Eq. 3) *versus* the Optronics OL-754 spectroradiometer. The coefficient of determination (r^2) was 0.99, the slope (95% CI) was 1.00 ± 0.01, and the y-intercept was 1.3 ± 1.0 μeinstein cm^{-2}. Note the change in y-scale in panels (A) and (B). The slopes and y-intercepts were determined from correlation analysis employing the Pearson major axis method (43).

Intercalibration study

Nitrate actinometer. Photon exposure measurements made using the nitrate actinometer were compared to photon exposures measurements made with the SERC SR-18 and the OL-754 instruments. The focus of the intercomparison study was primarily on the SERC SR-18 instrument because of its rapid response and spectral filtering for measuring UV-B irradiances. For comparison of instrumental data to the actinometer results, all instrumental data were converted from J cm^{-2} to einstein cm^{-2}.

Photon exposures that were determined from SA and pHBA production using Eq. 3 in the nitrate actinometer during the winter/spring study showed excellent agreement with photon exposures measured by the SERC SR-18 instrument (Fig. 6). Correlation analysis (*vide supra*) of these data for SA (Fig. 6A) yielded a slope (95% CI) of 0.98 ± 0.01, with a y-intercept (95% CI) of 0.14 ± 0.14 μeinstein cm^{-2} ($n = 57$, $r^2 = 0.99$), while analysis of the same plot for pHBA (data not shown) yielded a slope (95% CI) of 0.94 ± 0.02 and a y-intercept (95% CI) of −0.13 ± 0.24 μeinstein cm^{-2} ($n = 57$, $r^2 = 0.98$). Although these slopes are significantly different from the predicted slope of 1.0 at the 95% confidence level, the difference is quite small and does not take into account errors associated with calibration of the SR-18 radiometer. Taking into account the absolute uncertainty in

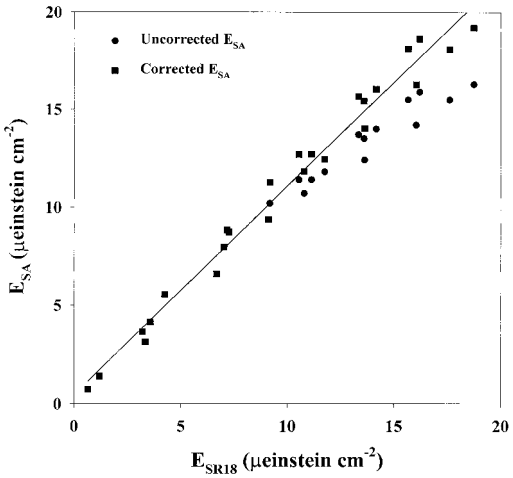

Figure 7. Photon exposure from 311 to 333 nm determined from SA production in the nitrate actinometer using Eq. 3 (●) and Eq. 5 (■) correlated with photon exposures obtained using the SERC SR-18 radiometer. The best-fit line through the corrected data was determined from correlation analysis employing the Pearson major axis method (43). The coefficient of determination (r^2) was 0.98, the slope (95% CI) was 1.06 ± 0.06, and the y-intercept was 0.44 ± 0.71 μeinstein cm^{-2}.

calibrating radiometers and spectroradiometers (*ca* 4–5% (17,47)), the nitrate actinometer and the SR-18 are in excellent agreement.

Although excellent agreement was shown between the SERC SR-18 radiometer and the nitrate actinometer based on either SA or on pHBA production, photon exposures should be based on SA production, except for long-term irradiations where significant photolysis of SA is expected. The quantification of SA is recommended for shorter irradiations because its detection by fluorescence is inherently more sensitive than the detection of pHBA by absorbance. High sensitivity is required for very low photon exposure measurements (*i.e.* at the 0.1% light level in the water column, or during short deployments).

As previously discussed, SA undergoes photodegradation in sunlight, which becomes important for long irradiations. This effect is evident in the correlation of the photon exposure determined by the nitrate actinometer to that determined by the OL-754 spectroradiometer (Fig. 7). When SA degradation is not taken into account, the response of the actinometer demonstrates curvature at high photon exposures due to the photolysis of SA (Fig. 7). The decrease in response of the SA-based nitrate actinometer was not evident in the SERC SR-18 intercalibration study (Fig. 6A) because photon exposures were approximately 65% lower due to weather conditions and seasonal effects.

When the results shown in Fig. 7 are corrected for SA degradation employing Eq. 5 (*vide supra*), linear results are obtained (Fig. 7). Correlation analysis of the corrected plot yielded a slope (95% CI) of 1.06 ± 0.06, with a y-intercept (95% CI) of 0.44 ± 0.71 μeinstein cm^{-2} (n = 25, r^2 = 0.98). Nonlinearity was not observed for the pHBA-based nitrate actinometer when it was correlated to the OL-754 (data not shown). Correlation analysis of pHBA data yielded a slope (95% CI) of 1.02 ± 0.03 and a y-intercept (95% CI) of 0.32 ± 0.68 μeinstein cm^{-2} (n = 25, r^2 = 0.97). For all intercomparisons, the y-intercept was not significantly different from zero at the 95% confidence level.

Nitrite actinometer. Photon exposure measurements made using the Mylar D-filtered nitrite actinometer were compared to photon exposure measurements made with the OL-754 spectroradiometer over the nitrite actinometer response bandwidth (330–380 nm). The photon exposure determined from SA or pHBA production in the 1 m*M* nitrite actinometer was determined from Eq. 3 using the mean values for the molar absorption coefficient and quantum yields over the response bandwidth of the Mylar D-filtered nitrite actinometer (Table 3). The photon exposure determined using the nitrite actinometer agreed very well with the photon exposure determined by the OL-754 (Fig. 6B). From correlation analysis of these data, the nitrite actinometer with SA detection had a response (95% CI) of 1.00 ± 0.01 (n = 47, r^2 = 0.99) relative to the OL-754, with a y-intercept (95% CI) of 1.3 ± 1.0 μeinstein cm^{-2}, while linear correlation analysis of the plot of photon exposure based on pHBA production in the nitrite actinometer *versus* the OL-754 yielded a slope (95% CI) of 1.00 ± 0.02, with a y-intercept (95% CI) of −0.35 ± 0.43 μeinstein cm^{-2} (n = 44, r^2 = 0.99) (data not shown).

Detection limit

The lower detection limit of the method is approximately 5 × 10^{-9} einstein cm^{-2} at 25°C, based on a detection limit for SA production by HPLC analysis of 0.5 n*M*. The upper detection limit was not investigated in this study, but it should be ultimately dictated by fouling of the quartz tubes during long-term (multiday) deployments in natural waters. Additionally, the upper detection limit may be limited by significant loss of NO_x^- or by side reactions arising from appreciable buildup of products.

DISCUSSION

Photon exposures determined using nitrate and nitrite actinometers were in excellent agreement with the instrumentally determined photon exposures. In general, comparisons of the actinometers to the instruments yielded slopes that were not significantly different from one, and y-intercepts that were not significantly different from zero at the 95% confidence level. These results demonstrate that the nitrate and nitrite actinometers provide an excellent technique to determine photon exposures in the UV component of the solar spectrum. They are particularly well suited for underwater measurements and can be deployed in an array to provide spatial quantification of photon exposures in aquatic systems. These actinometers have been used successfully in two field studies in Antarctica, with results of these studies presented elsewhere (48).

In addition to their excellent agreement with spectroradiometers, the actinometers provide several benefits over currently used actinometers and dosimeters for characterizing UV radiation. First, no adjustments to the actinometer solutions (*i.e.* no quenchers or sensitizers) are needed for long or short-term deployments. Second, the actinometers are very sensitive and capable of quantifying photon exposures below the 0.1% UV light level in the water column. Third, SA can be quantified using batch fluorescence (*i.e.* no HPLC

needed), allowing for rapid field analysis (39). Finally, irradiated actinometer solutions are very stable under refrigeration, allowing for analysis in the home laboratory, with no need for analytical equipment in the field (39). Based on these advantages, these actinometers can serve as a valuable method for the quantitative comparison of field-based photochemical and photobiological rates determined by different investigators.

Acknowledgements—We would like to thank Drs. John P. Hassett and David L. Johnson (SUNY ESF), William L. Miller (Dalhousie University) and Richard G. Zepp (U.S. Environmental Protection Agency, Athens, GA) for discussions regarding the actinometers and this manuscript. Financial support for this project was provided by the National Science Foundation to David J. Kieber (OPP-9610173 and OCE-9711174) and Kenneth Mopper (OPP-9527255 and OCE-9711206).

REFERENCES

1. Kieber, D. J. (2000) Photochemical production of biological substrates. In *The Effects of UV Radiation in the Marine Environment*, Chap. 5 (Edited by S. J. de Mora, S. Demers and M. Vernet), pp. 130–148. Cambridge University Press, Cambridge.
2. Mopper, K. and D. J. Kieber (2000) Marine photochemistry and its impact on carbon cycling. In *The Effects of UV Radiation in the Marine Environment*, Chap. 4 (Edited by S. J. de Mora, S. Demers and M. Vernet), pp. 101–129. Cambridge University Press, Cambridge.
3. Zepp, R. G., T. V. Callaghan and D. J. Erickson (1995) Effects of increased solar ultraviolet radiation on biogeochemical cycles. *Ambio* **24**, 181–187.
4. Mims, F. M. (1994) Cumulus clouds and UV-B. *Nature* **371**, 291.
5. Nemeth, P., Z. Toth and Z. Nagy (1996) Effect of weather conditions on UV-B radiation reaching the Earth's surface. *J. Photochem. Photobiol. B: Biol.* **32**, 177–181.
6. Kirk, J. T. O. (1994) *Light and Photosynthesis in Aquatic Ecosystems*. Cambridge University Press, Cambridge.
7. Josefsson, W. A. P. (1993) Monitoring Ultraviolet Radiation. In *Environmental UV Photobiology* (Edited by A. R. Young, L. O. Björn, J. Moan and W. Nultsch), pp. 73–88. Plenum Press, New York.
8. Crutzen, P. J. (1992) Ultraviolet on the increase. *Nature* **356**, 104–105.
9. Davies-Colley, R. J. and W. N. Vant (1987) Absorption of light by yellow substance in freshwater lakes. *Limnol. Oceanogr.* **32**, 416–425.
10. Kirk, J. T. O. (1994) Optics of UV-B radiation in natural waters. *Arch. Hydrobiol. Ergebn. Limnol.* **43**, 1–16.
11. Laurion, I., W. F. Vincent and D. R. S. Lean (1997) Underwater ultraviolet radiation: development of spectral models for northern high latitude lakes. *Photochem. Photobiol.* **65**, 107–114.
12. Smith, R. C. and J. E. Tyler (1976) Transmission of solar radiation into natural waters. In *Photochemical and Photobiological Reviews* (Edited by R. C. Smith), pp. 117–155. Plenum Press, New York.
13. Williamson, C. E., R. S. Stemberger, D. P. Morris, T. M. Frost and S. G. Paulsen (1996) Ultraviolet radiation in North American lakes: attenuation estimates from DOC measurements and implications for plankton communities. *Limnol. Oceanogr.* **41**, 1024–1034.
14. Scully, N. M. and D. R. S. Lean (1994) The attenuation of ultraviolet radiation in temperate lakes. *Arch. Hydrobiol. Ergebn. Limnol.* **43**, 135–144.
15. Tüg, H. and M. E. M. Baumann (1994) Problems of UV-B radiation measurements in biological research. Critical remarks on current techniques and suggestions for improvements. *Geophys. Res. Lett.* **21**, 689–692.
16. Verhoeven, J. W. (1996) Glossary of terms used in photochemistry (IUPAC recommendations 1996). *Pure Appl. Chem.* **68**, 2223–2286.
17. Thompson, A., E. A. Early, J. DeLuisi, P. Disterhoft, D. Wardle, J. Kerr, J. Rives, Y. Sun, T. Lucas, T. Mestechkina, and P. Neale (1997) The 1994 North American interagency intercomparison of ultraviolet monitoring spectroradiometers. *J. Res. Natl. Inst. Stand. Technol.* **102**, 279–320.
18. DeLuisi, J. J. and J. M. Harris (1983) A determination of the absolute radiant energy of a Robertson–Berger meter sunburn unit. *Atmos. Environ.* **17**, 751–758.
19. Berger, D. S. (1976) The sunburning ultraviolet meter: design and performance. *Photochem. Photobiol.* **24**, 587–593.
20. Johnsen, B. and J. Moan (1991) The temperature sensitivity of the Robertson–Berger sunburn meter, model 500. *J. Photochem. Photobiol. B: Biol.* **11**, 277–284.
21. Dulin, D. and T. Mill (1982) Development and evaluation of sunlight actinometers. *Environ. Sci. Technol.* **16**, 815–820.
22. Zepp, R. G., M. M. Gumz, W. L. Miller and H. Gao (1998) Photoreaction of valerophenone in aqueous solution. *J. Phys. Chem.* **102**, 5716–5723.
23. Rahn, R. and M. A. Lee (1998) Iodouracil as a personal dosimeter for solar UVB. *Photochem. Photobiol.* **68**, 173–178.
24. Fleischmann, E. M. (1989) The measurement and penetration of ultraviolet radiation into tropical marine water. *Limnol. Oceanogr.* **34**, 1623–1629.
25. Regan, J. D. and H. Yoshida (1995) DNA UVB dosimeters. *J. Photochem. Photobiol. B: Biol.* **31**, 57–61.
26. Boelen, P., I. Obernosterer, A. A. Vink and A. G. J. Buma (1999) Attenuation of biologically effective UV radiation in tropical Atlantic waters measured with a biochemical DNA dosimeter. *Photochem. Photobiol.* **69**, 34–40.
27. Munakata, N. (1993) Biologically effective dose of solar ultraviolet radiation estimated by spore dosimetry in Tokyo since 1980. *Photochem. Photobiol.* **58**, 386–392.
28. Ronto, G., S. Gáspár P. Gróf, A. Bérces and Z. Gugolya (1994) Ultraviolet dosimetry in outdoor measurements based on bacteriophage T7 as a biosensor. *Photochem. Photobiol.* **59**, 209–214.
29. Daniels, M., R. V. Meyers and E. V. Belardo (1968) Photochemistry of the aqueous nitrate system. I. Excitation in the 300-mμ band. *J. Phys. Chem.* **72**, 389–399.
30. Zafiriou, O. C. and M. B. True (1979) Nitrate photolysis in seawater by sunlight. *Mar. Chem.* **8**, 33–42.
31. Zepp, R. G., J. Hoigné and H. Bader (1987) Nitrate-induced photooxidation of trace organic chemicals in water. *Environ. Sci. Technol.* **21**, 443–450.
32. Zellner, R., M. Exner and H. Herrmann (1990) Absolute hydroxy radical quantum yields in the laser photolysis of nitrate, nitrite and dissolved hydrogen peroxide at 308 and 351 nm in the temperature range 278–353 K. *J. Atmos. Chem.* **10**, 411–425.
33. Warneck, P. and C. Wurzinger (1988) Product quantum yields for the 305-nm photodecomposition of NO_3^- in aqueous solution. *J. Phys. Chem.* **92**, 6278–6283.
34. Mark, G., H. G. Korth, H. P. Schuchmann and C. von Sonntag (1996) The Photochemistry of aqueous nitrate ion revisited. *J. Photochem. Photobiol. A: Chem.* **101**, 89–103.
35. Strickler, S. J. and M. Kasha (1963) Solvent effects on the electronic absorption spectrum of nitrite ion. *J. Am. Chem. Soc.* **85**, 2899–2901.
36. Treinin, A. and E. Hayon (1970) Absorption spectra and reaction kinetics of NO_2, N_2O_3, and N_2O_4 in aqueous solution. *J. Am. Chem. Soc.* **92**, 5821–5828.
37. Zafiriou, O. C. and R. Bonneau (1987) Wavelength-dependent quantum yield of OH radical formation from photolysis of nitrite ion in water. *Photochem. Photobiol.* **45**, 723–727.
38. Zhou, X. and K. Mopper (1990) Determination of photochemically produced hydroxyl radicals in seawater and freshwater. *Mar. Chem.* **30**, 71–88.
39. Jankowski, J. J., D. J. Kieber and K. Mopper (1999) Nitrate and nitrite ultraviolet actinometers. *Photochem. Photobiol.* **70**, 319–328.
40. Hatchard, C. G. and C. A. Parker (1956) A new sensitive chemical actinometer. II. Potassium ferrioxalate as a standard chemical actinometer. *Proc. R. Soc.* **235A**, 518–536.
41. Early, E., A. Thompson, C. Johnson, J. DeLuisi, P. Disterhoft, D. Wardle, E. Wu, W. Mou, Y. Sun, T. Lucas, T. Mestechkina,

L. Harrison, J. Berndt and D. S. Hayes (1998) The 1995 North American interagency intercomparison of ultraviolet monitoring spectroradiometers. *J. Res. Natl. Inst. Stand. Technol.* **103**, 15–62.
42. Kieber, D. J., B. H. Yocis and K. Mopper (1997) Free-floating drifter for photochemical studies in the water column. *Limnol. Oceanogr.* **42**, 1829–1833.
43. York, D. (1966) Least-squares fitting of a straight line. *Can. J. Phys.* **44**, 1079–1086.
44. Zepp, R. G. and D. M. Cline (1977) Rates of direct photolysis in aquatic environment. *Environ. Sci. Technol.* **11**, 359–366.
45. Gaffney, J. S., N. A. Marley and M. M. Cunningham (1992) Measurement of the absorption constants for nitrate in water between 270 and 335 nm. *Environ. Sci. Technol.* **26**, 207–209.
46. Zuo, Y. and Y. Deng (1998) The near UV absorption constants for nitrite ion in aqueous solution. *Chemosphere* **36**, 181–188.
47. Leszczynski, K., K. Jokela, L. Ylianttila, R. Visuri and M. Blumthaler (1998) Erythemally weighted radiometers in solar UV monitoring: results from the WMO/STUK intercomparison. *Photochem. Photobiol.* **67**, 212–221.
48. Jankowski, J. J. (1999) The Development and Application of Ultraviolet Solar Actinometers. Ph.D. thesis, State University of New York, College of Environmental Science and Forestry, Syracuse, NY. 170 pp.